Thickness-induced crossover from strong to weak collective pinning in exfoliated $FeTe_{0.6}Se_{0.4}$ thin films at 1 T

Ryoya Nakamura,[1] Masashi Tokuda,[1] Mori Watanabe,[1] Masamichi Nakajima,[1] Kensuke Kobayashi,[1,2] and Yasuhiro Niimi[1,3,*]

[1]*Department of Physics, Graduate School of Science, Osaka University, Toyonaka 560-0043, Japan*
[2]*Institute for Physics of Intelligence and Department of Physics, Graduate School of Science, The University of Tokyo, Tokyo 113-0033, Japan*
[3]*Center for Spintronics Research Network, Osaka University, Toyonaka 560-8531, Japan*

(Received 16 July 2021; revised 26 September 2021; accepted 7 October 2021; published 14 October 2021)

We studied flux pinning in exfoliated $FeTe_{0.6}Se_{0.4}$ thin-film devices with a thickness d from 30 to 150 nm by measuring the critical current density J_c. In bulk $FeTe_{0.6}Se_{0.4}$, the flux pinning has been discussed in the framework of weak collective pinning, while there is little knowledge on the pinning mechanism in the thin-film region. From the thickness d dependence of J_c at a fixed magnetic field of 1 T, we found that the strong pinning is dominant below $d \approx 70$ nm, while the weak collective pinning becomes more important above $d \approx 100$ nm. This crossover thickness can be explained by the theoretical model proposed by van der Beek *et al.* [Phys. Rev. B **66**, 024523 (2002)].

DOI: 10.1103/PhysRevB.104.165412

I. INTRODUCTION

Since 2008, iron-based superconductors (IBSs) have been well studied as a new group of high-temperature superconductors because of the two-dimensional layered structure similar to cuprate superconductors [1]. Their fundamental properties such as the short coherence length and large upper-critical field are useful for superconducting wires [2]. For such applications, it is essential to increase the critical current density J_c. In order to achieve this, the pinning mechanism of magnetic vortices needs to be clarified.

Among all kinds of IBSs, the iron-based chalcogenide $FeTe_{1-x}Se_x$ with $x = 0.4 \sim 0.5$ (FTS) has the simplest crystal structure with only Fe*Ch* (*Ch* = Se or Te) layers. There have been many reports on bulk [3–12] and thin-film [13–16] FTS single crystals, which enable a detailed discussion of the pinning mechanism. Although the critical temperature T_c is not so high, the upper critical field is comparable to other IBSs. Thus, FTS has a potential to replace low-temperature superconducting wires such as Nb-Ti superconductors. In addition, FTS is a candidate for topological superconductor. Particularly it has been intensively studied on the detection of zero energy vortex bound state (ZVBS) in magnetic vortices, which is a fingerprint of the Majorana quasiparticles [17–20]. In fact, a recent scanning tunneling microscopy study demonstrated the existence of ZVBS in magnetic vortices [19]. Simultaneously, however, it also revealed that some of the magnetic vortices do not contain the ZVBS. This suggests that the Majorana zero modes gain finite energies via the interaction between magnetic vortices, resulting in an energy splitting of the zero modes. In order to unveil the ZVBS in the superconducing FTS, it is helpful to understand the magnetic vortex lattice and also its pinning mechanism under finite magnetic fields.

In general, there are two pinning mechanisms in superconductors, i.e., weak collective pinning [21,22] and strong pinning [23,24]. In the former case, the pinning stems from the atomic-scale inhomogeneity of the superconducting regions due to impurities or defects and is further categorized into two types. One is δl pinning, originating from spatial fluctuations of the mean-free-path l due to lattice defects [21]. This is related to the derivative of the macroscopic wave function in the Ginzburg-Landau theory. The other is δT_c pinning, originating from spatial fluctuations of the critical temperature T_c [21]. This is related to the fact that the coefficient α of the probability density for the macroscopic wave function in the Ginzburg-Landau theory is proportional to $T_c - T$. For FTS single crystals, the pinning mechanisms have been determined by analyzing magnetization measurements with the Bean model [4–8]. In most cases, the δl pinning is dominant [4–6], while in some cases both the δl and δT_c pinnings coexist [7,8].

Contrary to the weak collective pinning, the strong pinning takes place at large-sized defects comparable to the coherence length ($\approx$10 nm) and can induce a high critical current density [25,26]. It has been established that the strong pinning is a dominant mechanism for 100–300 nm thick $YBa_2Cu_3O_{7-x}$ (YBCO) films where the critical current density has a large value [24,27]. Although there are some reports on enhanced critical current densities [28–30] as well as strong pinning [31–33] in IBS thin films, the relation between the strong pinning and the thickness of IBSs has not been fully elucidated yet.

In this work, we directly obtained J_c in exfoliated $FeTe_{0.6}Se_{0.4}$ thin-film devices with several different thicknesses d by measuring current-voltage properties at a fixed out-of-plane magnetic field of 1 T. For $d \lesssim 70$ nm, J_c linearly increases with increasing d. Such a tendency is consistent with the strong pinning reported in YBCO thin-film superconductors. When d exceeds $\approx$100 nm, J_c decreases with

*niimi@phys.sci.osaka-u.ac.jp

increasing d and eventually approaches the value estimated for bulk FTS. By plotting J_c as a function of d, we observe a crossover behavior from the strong pinning in thin-film regions to the weak collective pinning. This crossover thickness $d^* = 70 \sim 100$ nm can be explained by the theoretical model proposed by van der Beek *et al.* [24].

II. EXPERIMENTAL DETAILS

Single crystals of $FeTe_{0.6}Se_{0.4}$ were grown from a stoichiometric mixture of Fe, Te, and Se powder. We note that in the present work, $FeTe_{0.6}Se_{0.4}$ has been studied, but we use the same abbreviation (FTS) as for a general composition ratio $FeTe_{1-x}Se_x$ in this paper. The mixture was loaded into an alumina crucible and sealed in an evacuated quartz tube. The quartz tube was heated at 650°C for 10 h and then 1070°C for 15 h, followed by cooling down to 620°C at a rate of 3°C/h. FTS has a van-der-Waals interaction between the two adjacent *Ch* layers, which makes it easier to fabricate thin-film devices using the mechanical exfoliation technique. On the other hand, it has been known that excess Fe is present in between the *Ch* layers, which gives rise to magnetic correlations and suppresses the superconductivity [34]. To remove the excess Fe, we annealed as-grown FTS bulk crystals at 400°C for 40 h under 1% atmosphere of O_2 gas [35–37]. To determine T_c of FTS bulk crystals, we measured the dc magnetic susceptibility using Magnetic Property Measurement System (Quantum Design). Figure 1(a) shows the temperature dependence of the magnetic susceptibility χ for as-grown and annealed FTS. In this work, T_c^{bulk} is defined as a temperature where χ for zero-field cooling (ZFC) starts to decrease. From the χ measurements, we determine $T_c^{bulk} = 13.7$ K for the as-grown sample and $T_c^{bulk} = 14.4$ K for the annealed crystal. By annealing the FTS crystal, T_c^{bulk} has been enhanced by 5%, which is consistent with Refs. [35–37]. Hereafter we mainly focus on the annealed FTS unless otherwise noted, whereas we also use the as-grown FTS for comparison.

To obtain thin-film devices, we adopted the mechanical exfoliation technique using Scotch tape under ambient conditions. Some of the exfoliated FTS flakes onto the Scotch tapes were transferred to a thermally oxidized silicon substrate. We then coated polymethyl-methacrylate resist on the substrate and patterned electrodes with electron beam lithography. After the development of the resist, Ti (5 nm) and Au (150 nm) were deposited. Ti works as an adhesion layer for the Si/SiO_2 substrate. Before the deposition of electrodes, we performed Ar milling process for 55 s to remove the residual resist at the surface of FTS. In fact, we have confirmed the following: (1) This process does not give significant damage to FTS; (2) without the Ar milling process, we cannot obtain an Ohmic contact between FTS and the electrodes because of the residual resist at the interface. Figure 1(b) shows an optical microscope image of a typical device. The thickness d of FTS was determined with a commercially available atomic force microscopy after finishing transport measurements. Although we sometimes found not-perfectly homogeneous thin-film flakes, we regarded d as a film thickness when surface regions with d exceed 85%. In the present work, d ranges from 30 to 150 nm. Because of the limitation of the present exfoliation method, we could not obtain FTS devices thicker than 150 nm.

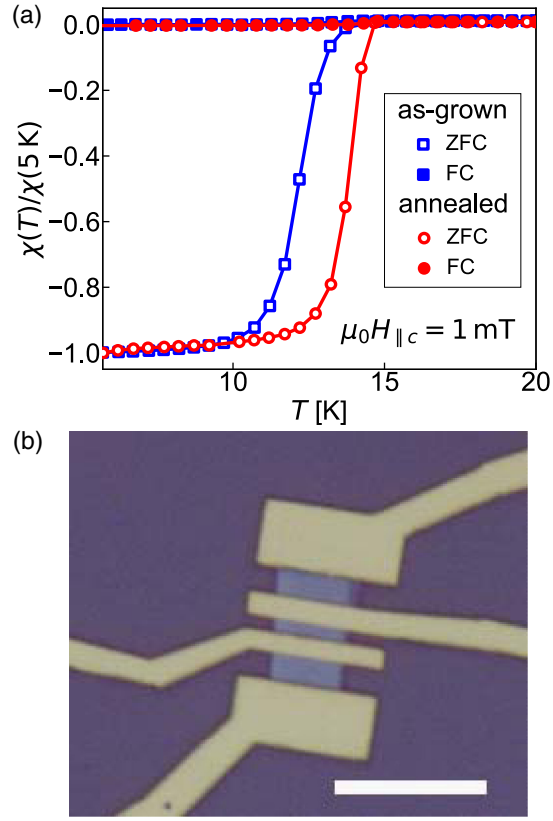

FIG. 1. (a) Temperature dependence of magnetic susceptibilities of as-grown bulk FTS (square) and annealed bulk FTS (circle) under the magnetic field ($\mu_0 H_{\|c}$) of 1 mT. The closed and open symbols indicate data obtained with field cooling (FC) and ZFC, respectively. The vertical axis is normalized by the data for ZFC at $T = 5$ K for each sample. (b) Optical microscope image of our typical device. The white scale bar corresponds to 10 μm.

We measured the resistivity ρ of thin-film FTS devices with a standard ac Lock-in technique. To determine J_c, we performed dc current (I)-voltage (V) measurements.

III. EXPERIMENTAL RESULTS

First, to determine T_c of FTS thin-film devices, we measured the temperature T dependence of the resistivity ρ in Fig. 2(a). When the film thickness d is larger than 100 nm, ρ decreases with decreasing T for the whole temperature region. Below $d \approx 100$ nm, on the other hand, ρ slightly increases with decreasing T, takes a maximum, and becomes zero at low temperatures. In particular, a 30 nm thick device shows insulating behavior down to 13 K. Such tendencies are due to the inhomogeneity of superconducting states in FTS crystals, as reported in Ref. [38]. The superconducting percolation network, which is strongly connected in bulk, gradually weakens with decreasing d. This results in weak superconductivity for thinner FTS film devices. Figure 2(b) shows the thickness dependence of T_c. There are two ways to define T_c: One is to use the initial rise of resistivity from zero (T_c^{zero}), and the other is to use the onset of resistivity drop in ρ-T curve (T_c^{on}) as indicated in Fig. 2(a). Since there is a finite voltage jump even just below T_c^{on} [see Fig. 3(a)],

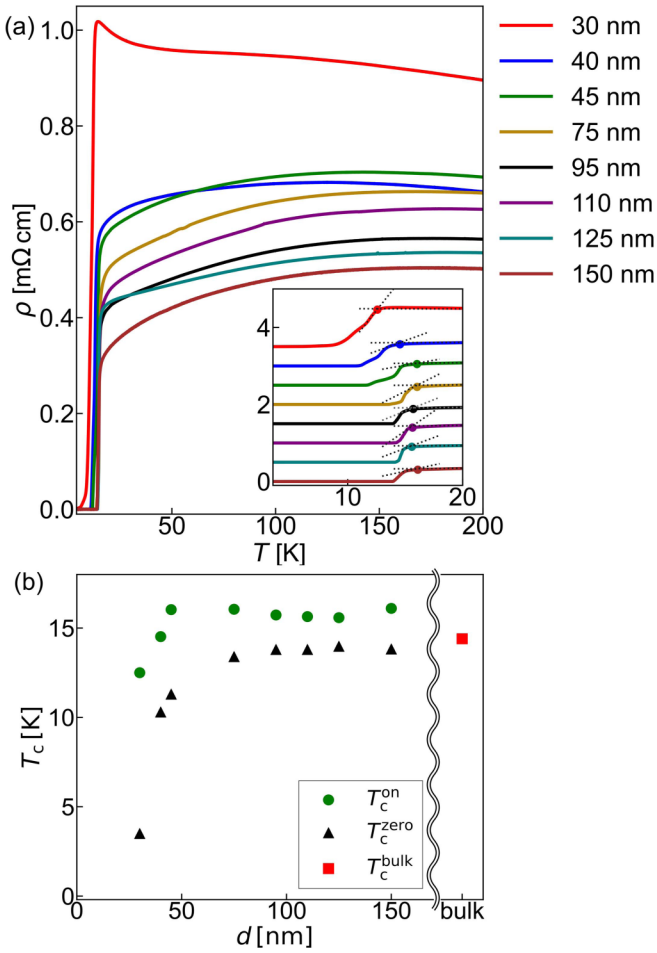

FIG. 2. (a) Temperature T dependence of ρ of FTS thin-film devices. The inset shows the close-up near T_c. We define two T_c, i.e., T_c^{zero} and T_c^{on}, as detailed in the main text. (b) Thickness d dependence of T_c^{zero} and T_c^{on}. We also plot T_c^{bulk} of annealed bulk FTS crystal for reference.

in this work we have adopted T_c^{on} as T_c, namely, $T_c \equiv T_c^{on}$. T_c starts to decrease below $d \lesssim 100$ nm and should vanish at $10 \sim 20$ nm. According to Ref. [36], the critical thickness d_0 below which T_c vanishes is 12 nm, which is consistent with the present work.

Next we performed I-V measurements under the out-of-plane magnetic field $\mu_0 H_{\parallel c} = 1$ T. Figure 3(a) shows dc current-voltage curves for a 95 nm thick FTS device at several different temperatures. We use the current density J instead of I to compare with different d devices. At low temperatures, there is a clear hysteresis that originates from the Joule heating in the FTS device. In the present work, we define J_c as the current density when the measured dc voltage exceeds a threshold value of 1 mV. For example, J_c is 0.78 MA/cm^2 at $T = 3$ K. In the vicinity of T_c, on the other hand, the hysteresis vanishes and the voltage jump near J_c becomes less clear. We also performed pulse current measurements with a pulse width of 1 ms and an interval of 100 ms in order to evaluate J_c without the effects of Joule heating. The obtained J_c was almost the same value as in Fig. 3(a). In Fig. 3(b), J_c obtained from Fig. 3(a) is plotted as a function of T. J_c monotonically decreases with increasing T and vanishes at T_c.

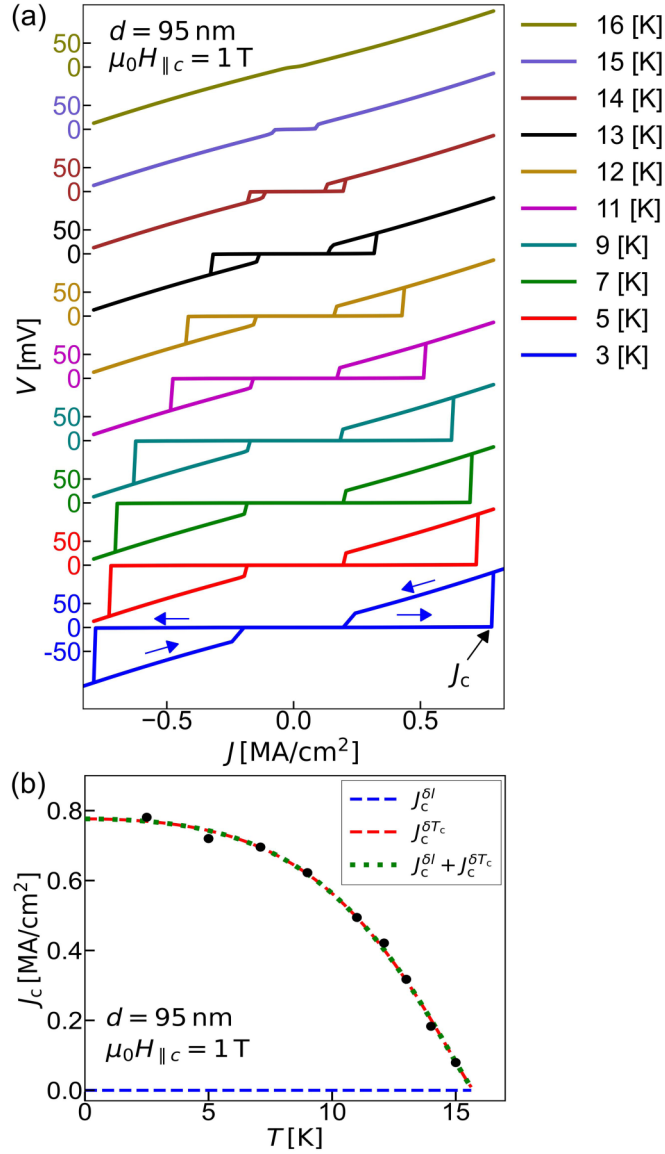

FIG. 3. (a) Current-voltage properties for $d = 95$ nm thick device under the out-of-plane magnetic field $\mu_0 H_{\parallel c} = 1$ T at various temperatures. (b) Temperature dependence of $J_c(T)$ for $d = 95$ nm thick device under the out-of-plane magnetic field $\mu_0 H_{\parallel c} = 1$ T. The green dotted line is the best fit with Eqs. (2)–(4), while the red and blue dashed lines are the contributions from δT_c and δl pinnings, respectively.

We also measured the magnetic field and angle dependences of J_c for the $d = 95$ nm thick FTS device at $T = 3$ K. Figure 4(a) shows J_c as a function of $\mu_0 H$ along the c axis and the ab plane. When the magnetic field is applied along the ab plane, J_c is more or less constant. For the perpendicular magnetic field ($\mu_0 H \parallel c$), on the other hand, J_c decreases with increasing $\mu_0 H$. Figure 4(b) shows J_c at $\mu_0 H = 1$ T as a function of the rotation angle θ from the c axis. $J_c(\theta)$ has a broad maximum at $\theta = 90°$ ($\mu_0 H \parallel ab$), and there is no peak at $\theta = 0°$ nor 180° ($\mu_0 H \parallel c$). If we assume that $J_c(\theta, \mu_0 H)$ depends only on the c axis component of the applied magnetic field, i.e., $\mu_0 H_{\parallel c} = \mu_0 H \cos\theta$, the angle dependence of J_c is expected as shown by the red curve, which is consistent with

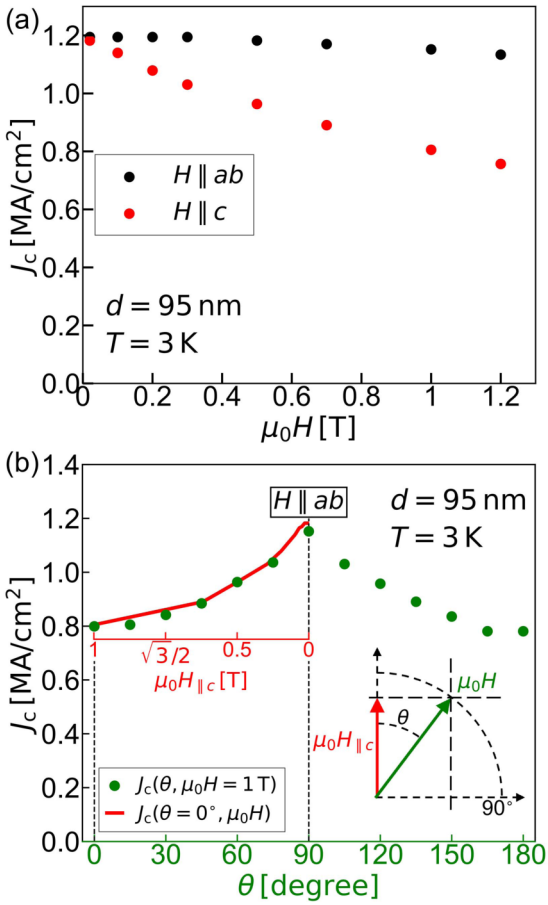

FIG. 4. (a) J_c of $d = 95$ nm thick device measured at $T = 3$ K as a function of $\mu_0 H$ along the *ab* plane (black circle) and the *c* axis (red circle). (b) J_c of $d = 95$ nm thick device measured at $T = 3$ K and $\mu_0 H = 1$ T as a function of angle θ from the *c* axis (green circle). We show the definitions of θ and $\mu_0 H$ in the inset. The magnetic field applied along the *ab* plane corresponds to $\theta = 90°$.

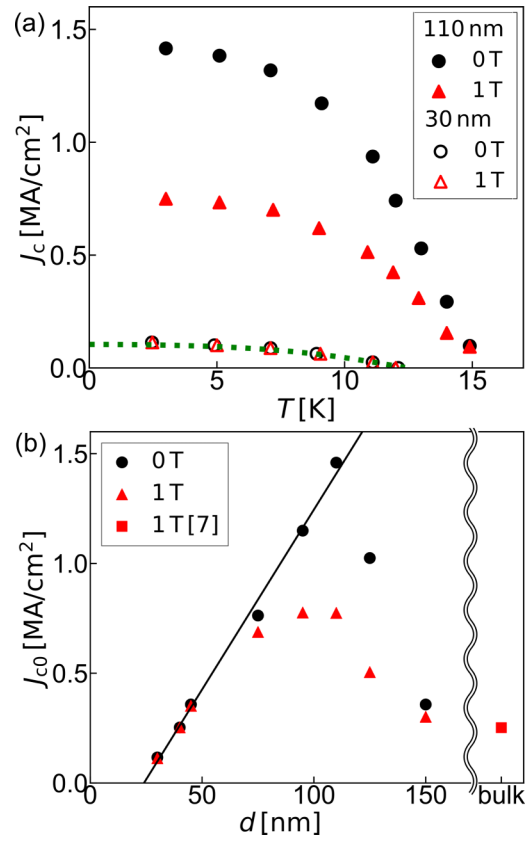

FIG. 5. (a) Temperature dependence of $J_c(T)$ at $\mu_0 H_{\parallel c} = 0$ T (black circles) and 1 T (red triangles) for $d = 30$ and 110 nm. The green dotted line is the best fit for $d = 30$ nm at $\mu_0 H_{\parallel c} = 0$ T using Eqs. (2)–(4). (b) Thickness dependence of J_{c0} for $\mu_0 H_{\parallel c} = 0$ T (black circles) and 1 T (red triangles). For comparison, we also plot J_c at $\mu_0 H_{\parallel c} = 1$ T for bulk FTS in Ref. [7] (red square). The solid line is the best fit with Eq. (1) for J_{c0} below $d = 50$ nm.

the experimental data. This clearly shows that J_c depends only on the perpendicular component of the magnetic field. Such magnetic field and angle dependences of J_c are consistent with previous works on FTS thin films [13–16].

Now we move on to the d dependence of J_c. In Fig. 5(a), we show the temperature dependence of $J_c(T)$ measured at $\mu_0 H_{\parallel c} = 0$ T and 1 T for $d = 30$ and 110 nm thick devices, respectively. There is almost no difference in $J_c(T)$ between 0 and 1 T for the 30 nm thick device, whereas the difference is significant for the 110 nm thick device. To see the d dependence of $J_c(T)$ at 0 and 1 T more systematically, we plot J_{c0}, which is obtained by extrapolating the $J_c(T)$ vs T curves down to $T = 0$ as detailed in the next section at $\mu_0 H_{\parallel c} = 0$ and 1 T. J_{c0} linearly increases with d up to $d \approx 70$ nm for 1 T and $d \approx 100$ nm for 0 T. Above $d \approx 100$ nm, J_{c0} suddenly decreases with increasing d and approaches a J_c value evaluated with the Bean model [7]. Figure 5(b) clearly indicates that there are two regions below $d \approx 70$ nm and above $d \approx 100$ nm; the former is the strong pinning region and the latter is the weak collective pinning region, as discussed in more detail in the next section.

IV. DISCUSSION

A. Strong pinning

We first discuss the strong pinning region below $d \approx 70$ nm. It is known that FTS is a highly inhomogeneous material [19,39–42]. According to electron energy loss spectroscopy measurements [42], there is an inhomogeneous distribution of Te in FTS crystals; it forms some clusters in FTS and the spatial variation of the cluster is approximately 10 nm. Therefore, the effect of the inhomogeneity should be prominent when d is of the order of 10 nm, where the strong pinning is more dominant [24,27].

Lower magnetic fields are favorable to confirm whether the strong pinning is essential in our thin-film FTS devices. This is because the vortex density in the low-field region is too small for weak collective pinning to contribute and only the strong pinning contributes to J_c [43]. Therefore, we measured J_c at $\mu_0 H = 0$ T (but probably with a small Oersted field). Then J_{c0}, J_c at $T = 0$ was obtained by fitting J_c vs T curves with some theoretical model. We first tried theoretical expressions discussed in Ref. [24] for the strong pinning, but none of them could reproduce our experimental data. Thus we adopted Eqs. (2)–(4) to fit the J_c vs T curves. We note that

Eqs. (2)–(4) are originally developed for the weak collective pinning region, as detailed in the next subsection. As shown in Fig. 5(a), J_c for the $d = 30$ nm thick device can be fitted with Eqs. (2)–(4). The evaluated J_{c0} does not depend on the applied magnetic field at least within 1 T and linearly increases with increasing d. In fact, these features cannot be explained by the weak collective theory but are consistent with the strong pinning theory, as detailed below. This fact also suggests that Eqs. (2)–(4) would be useful even for the strong pinning.

As mentioned above, J_{c0} at 0 T has the same value as at 1 T and linearly increases with d up to $d \approx 100$ nm [see Fig. 5(b)]. Such a d dependence of $J_c(d)$ has also been observed in YBCO films [24,27,44–46]. According to a theoretical model proposed by van der Beek *et al.* [24], the critical current density for very thin superconducting films is given by

$$J_{c0} = \frac{\varepsilon_0}{4\pi\,\Phi_0\xi_{ab}} \ln\left(1 + \frac{D_{ab}^2}{2\xi_{ab}^2}\right)\frac{D_c}{(d^* - d_0)^2}(d - d_0), \qquad (1)$$

where $\varepsilon_0 = (\Phi_0/4\pi\lambda_{ab})^2(4\pi/\mu_0)$ is the typical energy scale for single vortex, $\Phi_0 = h/2e$ is the flux quantum, λ_{ab} is the in-plane magnetic penetration depth at $T = 0$, $\mu_0 = 4\pi \times 10^{-7}$ H/m, ξ_{ab} is the in-plane coherence length at $T = 0$, and d_0 is the critical thickness where J_{c0} becomes zero. D_{ab} and D_c are the typical sizes of defect along the ab plane and c axis, respectively; d^* is the crossover film thickness from the very thin-film region to relatively thick-film region [24]. As described by Eq. (1), J_{c0} in the very thin-film region should be field-independent and linearly increases with increasing d. This is consistent with the d dependence of J_{c0} for $d \lesssim 70$ nm in Fig. 5(b), at least in the field range from 0 to 1 T. Furthermore, d_0 is also consistent with the thickness below which T_c vanishes in Fig. 2(b). The contribution of the strong pinning is more significant in this thickness range.

As we increase d further from 70 nm, a significant difference in J_{c0} is observed between $\mu_0 H = 0$ and 1 T. J_{c0} takes a maximum value at $d \approx 100$ nm for both magnetic fields and suddenly decreases with increasing d. This thickness range will be discussed in the next subsection. From the linear fitting for J_{c0} below $d \approx 70$ nm, we obtain the slope $J_{c0}/(d - d_0) \sim 1.6 \times 10^{17}$ A/m^3. By using $\xi_{ab} = 2.5$ nm [13], $\lambda_{ab} = 0.49$ μm [34] and assuming $D_{ab} = D_c = 10 \sim 20$ nm, we estimate the crossover film thickness d^* to be $70 \sim 110$ nm. This d^* value is consistent with the experimental crossover thickness ($70 \sim 100$ nm) shown in Fig. 5(b).

B. Weak collective pinning

It has been established that J_c in bulk FTS can be described by the weak collective pinning theory [21]. As shown in Fig. 5(b), J_c at 1 T in bulk FTS is very close to that in our thin-film devices with $d \gtrsim 100$ nm. Therefore, we analyze $J_c(T)$ using the weak collective pinning theory, as discussed for bulk FTS in previous works [4–8]. In the theoretical approach proposed by Griessen *et al.* [22], $J_c(T)$ in the moderately low-field region, where the strong pinning can be ignored and the motion of single vortex is essential, is given as

$$J_c^{\delta l}(t) = J_{c0}^{\delta l}(1 - t^2)^{5/2}(1 + t^2)^{-1/2} \qquad (2)$$

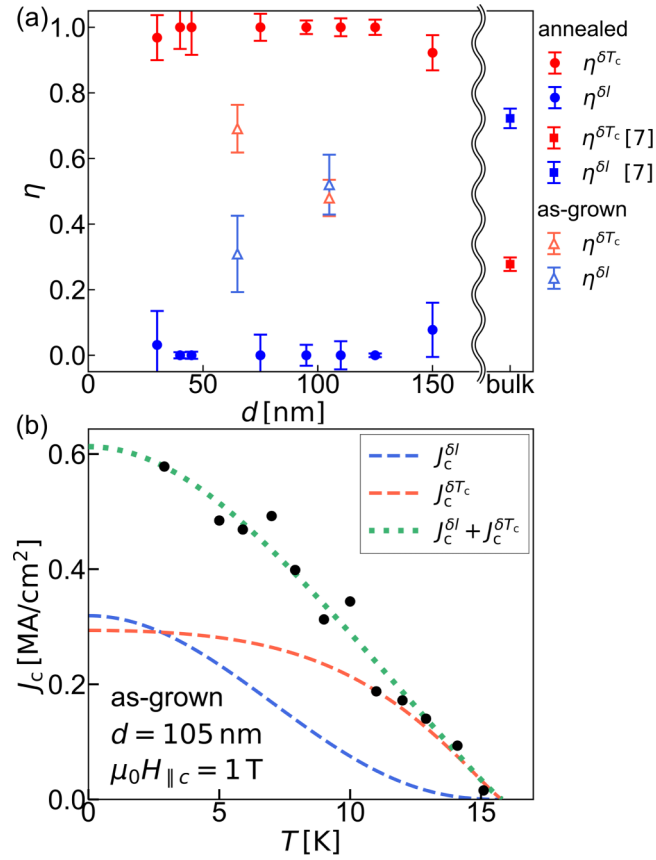

FIG. 6. (a) Thickness dependence of $\eta^{\delta l}$ (blue circles) and $\eta^{\delta T_c}$ (red circles) for annealed FTS samples. We also plot $\eta^{\delta l}$ (blue triangles) and $\eta^{\delta T_c}$ (red triangles) for as-grown FTS samples. For comparison, we also plot η for bulk FTS in Ref. [7] (square). (b) Temperature dependence of $J_c(T)$ for $d = 105$ nm thick as-grown device under the out-of-plane magnetic field $\mu_0 H_{\parallel c} = 1$ T. The green dotted line is the best fit with Eqs. (2)–(4), while the red and blue dashed lines are the contributions from δT_c and δl pinnings, respectively.

for δl pinning and

$$J_c^{\delta T_c}(t) = J_{c0}^{\delta T_c}(1 - t^2)^{7/6}(1 + t^2)^{5/6} \qquad (3)$$

for δT_c pinning; t is the reduced temperature ($t = T/T_c$). $J_{c0}^{\delta l}$ and $J_{c0}^{\delta T_c}$ are values at absolute zero temperature for δl pinning and δT_c pinning, respectively. If both pinning mechanisms coexist, J_c can be written as:

$$J_c(t) = J_c^{\delta l}(t) + J_c^{\delta T_c}(t). \qquad (4)$$

In Fig. 3(b), we show the best fit with Eqs. (2)–(4) for the 95 nm thick FTS device. We use two fitting parameters ($J_{c0}^{\delta l}$ and $J_{c0}^{\delta T_c}$) and obtain $J_{c0}^{\delta l} = 0 \pm 0.06$ MA/cm^2, $J_{c0}^{\delta T_c} = 0.77 \pm 0.03$ MA/cm^2, respectively. It is obvious that $J_{c0}^{\delta T_c}$ is much larger than $J_{c0}^{\delta l}$, indicating that the δT_c pinning is much more dominant. In Fig. 6(a), we show the thickness dependence of $\eta^{\delta l}$ ($\equiv J_{c0}^{\delta l}/J_{c0}$) and $\eta^{\delta T_c}$ ($\equiv J_{c0}^{\delta T_c}/J_{c0}$) obtained from fitting, where $J_{c0} = J_{c0}^{\delta l} + J_{c0}^{\delta T_c}$ is the total critical current density at $T = 0$. As mentioned in the previous subsection, the fitting with Eqs. (2)–(4) works even for the strong pinning region. In the present d range, $\eta^{\delta T_c}$ is much larger than $\eta^{\delta l}$, indicating that the δT_c pinning is more dominant. With increasing d,

the proportion of $\eta^{\delta l}$ becomes larger and exceeds that of $\eta^{\delta T_c}$ [7] in bulk FTS. This fact suggests that a crossover from the strong pinning to the weak collective pinning occurs at $d \approx 100$ nm.

Let us discuss the reason why the δT_c pinning is dominant in our thin-film devices. One possibility is the existence of excess Fe atoms. In most previous works on bulk FTS [4–6] where as-grown samples were used, the δl pinning is dominant. In such a case, a small amount of Fe impurities would be in between the two chalcogen layers. To remove the Fe impurities, Sun *et al.* performed oxygen annealing for FTS and found that both the δl and the δT_c pinnings coexist [7]. As mentioned in Sec. II, excess Fe (i.e., atomic-scale) impurities would be segregated at the surface of FTS by annealing it under an oxygen flow. This results in the reduction of the δl pinning contribution. To confirm the above scenario, we fabricated as-grown FTS thin-film devices and measured the temperature dependence of the critical current density in the same way as for annealed FTS devices. Figure 6(b) shows the temperature dependence of $J_c(T)$ for a 105 nm thick as-grown FTS device and also the result of fitting with Eqs. (2)–(4). When we measured I-V curves for as-grown devices, the critical current changed with every measurement. Therefore, the data points in Fig. 6(b) are scattered compared with those for the annealed FTS device shown in Fig. 3(b). From the fitting with Eqs. (2)–(4), $\eta^{\delta T_c}$ and $\eta^{\delta l}$ can be evaluated, as indicated by the triangle points in Fig. 6(a). The contribution of δl pinning is comparable to that of δT_c pinning, even at $d \approx 100$ nm where the latter is much more dominant than the former in the annealed devices. This clearly shows that the excess Fe plays an important role in the pinning mechanism in FTS. We note that even in as-grown FTS thin-film devices, the contribution of δT_c pinning is larger than that of the annealed bulk FTS sample.

Another possibility is the similarity between δT_c pinning and strong pinning. In the case of strong pinning at nanometer-sized defects, the δl pinning is less important than the δT_c pinning, as pointed out in Ref. [24]. This is because the scattering cross-section of quasiparticles at atomic-scale defects is negligibly small compared with that at large-sized defects. In thin-film FTS devices [42], the inhomogeneous distribution of Te would be more essential. Therefore, the contribution of the δT_c pinning is much more dominant in annealed FTS thin-film devices and is still large even in as-grown FTS thin-film devices which contain many atomic-scale defects. In bulk FTS, on the other hand, quasiparticles may scatter at atomic-scale defects and thus the δl pinning can be dominant because the path of the superconducting state is robust and the inhomogeneous distribution is not crucial [38].

V. CONCLUSION

We have studied the critical current density J_c in $FeTe_{0.6}Se_{0.4}$ (FTS) devices with thicknesses d from 30 to 150 nm by means of electric transport measurements. Below $d \approx 70$ nm, J_c does not depend on the applied magnetic field and linearly increases with increasing d. This result is consistent with the strong pinning theory. Above $d \approx 100$ nm, on the other hand, J_c decreases with increasing d and becomes comparable to that for bulk FTS, suggesting that the thicker film region corresponds to the weak collective pinning region. From these experimental results, a crossover from the strong pinning to the weak collective pinning is realized at $d^* = 70 \sim 100$ nm at a fixed magnetic field of 1 T. This value can be explained by the theoretical model where a defect size is comparable to the inhomogeneity of Te (≈10 nm) in FTS. Moreover, the δT_c pinning is much more dominant than the δl pinning in our thin-film devices. This is partly due to the fact that our FTS have been annealed under an oxygen flow before the exfoliation, resulting in a reduction of excess Fe (i.e., atomic-size impurities) in between the two chalcogen layers.

ACKNOWLEDGMENTS

This work was supported by JSPS KAKENHI (Grants No. JP16H05964, No. JP17K18756, No. JP19K21850, No. JP19H00656, No. JP19H05826, No. JP20H02557, No. JP20J20229, and No. JP21J20477), the Mazda Foundation, the Shimadzu Science Foundation, the Yazaki Memorial Foundation for Science and Technology, the SCAT Foundation, the Murata Science Foundation, Toyota Riken Scholar, the Kato Foundation for Promotion of Science, and the Asahi Glass foundation.

[1] Y. Kamihara, T. Watanabe, M. Hirano, and H. Hosono, J. Am. Chem. Soc. **130**, 3296 (2008).
[2] H. Hosono, A. Yamamoto, H. Hiramatsu, and Y. Ma, Mater. Today **21**, 278 (2018).
[3] B. C. Sales, A. S. Sefat, M. A. McGuire, R. Y. Jin, D. Mandrus, and Y. Mozharivskyj, Phys. Rev. B **79**, 094521 (2009).
[4] P. Das, A. D. Thakur, A. K. Yadav, C. V. Tomy, M. R. Lees, G. Balakrishnan, S. Ramakrishnan, and A. K. Grover, Phys. Rev. B **84**, 214526 (2011).
[5] M. Bonura, E. Giannini, R. Viennois, and C. Senatore, Phys. Rev. B **85**, 134532 (2012).
[6] A. Galluzzi, K. Buchkov, V. Tomov, E. Nazarova, A. Leo, G. Grimaldi, S. Pace, and M. Polichetti, Supercond. Sci. Technol. **33**, 094006 (2020).
[7] Y. Sun, T. Taen, Y. Tsuchiya, S. Pyon, Z. Shi, and T. Tamegai, Europhys. Lett. **103**, 57013 (2013).
[8] T. Tamegai, Y. Sun, T. Yamada, and S. Pyon, IEEE Trans. Appl. Supercond. **26**, 1 (2016).
[9] C. Yadav and P. Paulose, Solid State Commun. **151**, 216 (2011).
[10] D. Miu, T. Noji, T. Adachi, Y. Koike, and L. Miu, Supercond. Sci. Technol. **25**, 115009 (2012).
[11] M. Shahbazi, X. L. Wang, S. X. Dou, H. Fang, and C. T. Lin, J. Appl. Phys. **113**, 17E115 (2013).
[12] Z. F. Wu, Z. H. Wang, J. Tao, L. Qiu, S. G. Yang, and H. H. Wen, Supercond. Sci. Technol. **29**, 035006 (2016).
[13] K. Iida, J. Hänisch, E. Reich, F. Kurth, R. Hühne, L. Schultz, B. Holzapfel, A. Ichinose, M. Hanawa, I. Tsukada, M. Schulze, S. Aswartham, S. Wurmehl, and B. Büchner, Phys. Rev. B **87**, 104510 (2013).
[14] V. Braccini, S. Kawale, E. Reich, E. Bellingeri, L. Pellegrino, A. Sala, M. Putti, K. Higashikawa, T. Kiss, B.

Holzapfel, and C. Ferdeghini, Appl. Phys. Lett. **103**, 172601 (2013).
[15] P. Yuan, Z. Xu, Y. Ma, Y. Sun, and T. Tamegai, Supercond. Sci. Technol. **29**, 035013 (2016).
[16] H. Bryja, R. Hühne, K. Iida, S. Molatta, A. Sala, M. Putti, L. Schultz, K. Nielsch, and J. H änisch, Supercond. Sci. Technol. **30**, 115008 (2017).
[17] P. Zhang, K. Yaji, T. Hashimoto, Y. Ota, T. Kondo, K. Okazaki, Z. Wang, J. Wen, G. D. Gu, H. Ding, and S. Shin, Science **360**, 182 (2018).
[18] D. Wang, L. Kong, P. Fan, H. Chen, S. Zhu, W. Liu, L. Cao, Y. Sun, S. Du, J. Schneeloch, R. Zhong, G. Gu, L. Fu, H. Ding, and H. J. Gao, Science **362**, 333 (2018).
[19] T. Machida, Y. Sun, S. Pyon, S. Takeda, Y. Kohsaka, T. Hanaguri, T. Sasagawa, and T. Tamegai, Nat. Mater. **18**, 811 (2019).
[20] S. Zhu, L. Kong, L. Cao, H. Chen, M. Papaj, S. Du, Y. Xing, W. Liu, D. Wang, C. Shen, F. Yang, J. Schneeloch, R. Zhong, G. Gu, L. Fu, Y. Y. Zhang, H. Ding, and H. J. Gao, Science **367**, 189 (2020).
[21] G. Blatter, M. V. Feigel'man, V. B. Geshkenbein, A. I. Larkin, and V. M. Vinokur, Rev. Mod. Phys. **66**, 1125 (1994).
[22] R. Griessen, W. Hai-hu, A. J. J. van Dalen, B. Dam, J. Rector, H. G. Schnack, S. Libbrecht, E. Osquiguil, and Y. Bruynseraede, Phys. Rev. Lett. **72**, 1910 (1994).
[23] Y. N. Ovchinnikov and B. I. Ivlev, Phys. Rev. B **43**, 8024 (1991).
[24] C. J. van der Beek, M. Konczykowski, A. Abal'oshev, I. Abal'osheva, P. Gierlowski, S. J. Lewandowski, M. V. Indenbom, and S. Barbanera, Phys. Rev. B **66**, 024523 (2002).
[25] W. K. Yeoh, J. Horvat, S. X. Dou, and V. Keast, Supercond. Sci. Technol. **17**, S572 (2004).
[26] Z. Chen, F. Kametani, Y. Chen, Y. Xie, V. Selvamanickam, and D. C. Larbalestier, Supercond. Sci. Technol. **22**, 55013 (2009).
[27] A. O. Ijaduola, J. R. Thompson, R. Feenstra, D. K. Christen, A. A. Gapud, and X. Song, Phys. Rev. B **73**, 134502 (2006).
[28] P. Mele, K. Matsumoto, K. Fujita, Y. Yoshida, T. Kiss, A. Ichinose, and M. Mukaida, Supercond. Sci. Technol. **25**, 84021 (2012).
[29] W. Si, S. J. Han, X. Shi, S. N. Ehrlich, J. Jaroszynski, A. Goyal, and Q. Li, Nat. Commun. **4**, 1347 (2013).
[30] J. Lee, J. Jiang, F. Kametani, M. J. Oh, J. D. Weiss, Y. Collantes, S. Seo, S. Yoon, C. Tarantini, Y. J. Jo, E. E. Hellstrom, and S. Lee, Supercond. Sci. Technol. **30**, 85006 (2017).
[31] K. Iida, J. Hänisch, S. Trommler, V. Matias, S. Haindl, F. Kurth, I. L. del Pozo, R. Hühne, M. Kidszun, J. Engelmann, L. Schultz, and B. Holzapfel, Appl. Phys. Express **4**, 013103 (2010).
[32] Y. Zhang, C. T. Nelson, S. Lee, J. Jiang, C. W. Bark, J. D. Weiss, C. Tarantini, C. M. Folkman, S.-H. Baek, E. E. Hellstrom, D. C. Larbalestier, C.-B. Eom, and X. Pan, Appl. Phys. Lett. **98**, 042509 (2011).
[33] E. Bellingeri, S. Kawale, I. Pallecchi, A. Gerbi, R. Buzio, V. Braccini, A. Palenzona, M. Putti, M. Adamo, E. Sarnelli, and C. Ferdeghini, Appl. Phys. Lett. **100**, 082601 (2012).
[34] M. Bendele, S. Weyeneth, R. Puzniak, A. Maisuradze, E. Pomjakushina, K. Conder, V. Pomjakushin, H. Luetkens, S. Katrych, A. Wisniewski, R. Khasanov, and H. Keller, Phys. Rev. B **81**, 224520 (2010).
[35] Y. Sun, T. Taen, Y. Tsuchiya, Z. X. Shi, and T. Tamegai, Supercond. Sci. Technol. **26**, 015015 (2013).
[36] Y. Sun, Y. Tsuchiya, T. Taen, T. Yamada, S. Pyon, A. Sugimoto, T. Ekino, Z. Shi, and T. Tamegai, Sci. Rep. **4**, 4585 (2014).
[37] Y. Sun, Z. Shi, and T. Tamegai, Supercond. Sci. Technol. **32**, 103001 (2019).
[38] C. Yue, J. Hu, X. Liu, A. M. Sanchez, Z. Mao, and J. Wei, ACS Nano **10**, 429 (2016).
[39] B. Joseph, A. Iadecola, A. Puri, L. Simonelli, Y. Mizuguchi, Y. Takano, and N. L. Saini, Phys. Rev. B **82**, 20502(R) (2010).
[40] H. Hu, J.-M. Zuo, J. Wen, Z. Xu, Z. Lin, Q. Li, G. Gu, W. K. Park, and L. H. Greene, New J. Phys. **13**, 53031 (2011).
[41] U. R. Singh, S. C. White, S. Schmaus, V. Tsurkan, A. Loidl, J. Deisenhofer, and P. Wahl, Phys. Rev. B **88**, 155124 (2013).
[42] Y. Zhu, L. Chen, J. Ciston, and H. Wang, J. Phys. Chem. C **117**, 7170 (2013).
[43] C. J. van der Beek, G. Rizza, M. Konczykowski, P. Fertey, I. Monnet, T. Klein, R. Okazaki, M. Ishikado, H. Kito, A. Iyo, H. Eisaki, S. Shamoto, M. E. Tillman, S. L. Bud'ko, P. C. Canfield, T. Shibauchi, and Y. Matsuda, Phys. Rev. B **81**, 174517 (2010).
[44] E. Sheriff, R. Prozorov, Y. Yeshurun, A. Shaulov, G. Koren, and C. Chabaud-Villard, J. Appl. Phys. **82**, 4417 (1997).
[45] X. Wang and J. Z. Wu, Phys. Rev. B **76**, 184508 (2007).
[46] Y. V. Cherpak, V. L. Svetchnikov, A. V. Semenov, V. O. Moskaliuk, C. G. Tretiatchenko, V. S. Flis, and V. M. Pan, J. Phys.: Conf. Ser. **97**, 012259 (2008).